Axial Mixing in Modern Packings, Gas, and Liquid Phases: II. Two-Phase Flow

Ricardo Macías-Salinas and James R. Fair
Separations Research Program, Dept. of Chemical Engineering, The University of Texas at Austin, Austin, TX 78712

Axial mixing measurements of air and water under two-phase flow conditions were made in a large-scale packed column (0.43 m diameter) using tracer experiments. Part I of this article dealt with single-phase mixing in the same column, with the same internals. Four packings were studied: 25.4-mm ceramic Raschig rings, 25.4-mm metal Pall rings, Sulzer BX structured packing, and Flexipac 2 structured packing. Air and water flowed countercurrently through the column at atmospheric pressure and at gas rates varying from 0.25 kg/m^2· s up to the flooding point, and liquid rates from 3.25 to 8.5 kg/m^2· s. A diffusion-type model served to reproduce the experimental response curves obtained for both phases. The results confirmed previous observations for first-generation packings: axial mixing in the gas increases with both gas and liquid rates, whereas liquid-phase axial mixing is a decreasing function of liquid rate and is insensitive to gas rate up to the flooding point. It was also found that the BX packing produces the least mixing in both phases. The largest mixing effects in the gas phase are found for the Raschig rings, and the largest mixing effects for the liquid phase are found for Flexipac 2. Correlations were developed to reproduce the results, yielding an average ± 22% difference between experimental and correlated data.

Introduction

An important nonsegregated flow behavior, known as axial mixing, can occur in countercurrent, two-phase flow columns containing packing elements. This mixing represents a deviation from plug flow and is the result of the combined effect of various nonideal flow situations: channeling or backflow with some transverse mixing as well as backflow with infinite cross-mixing. In partially destroying the countercurrent contacting scheme of the flowing phases, this mixing adversely influences the axial concentration profile in the flowing streams, causing a decrease of mass-transfer driving forces and in consequence a drop in separation efficiency.

Axial mixing in countercurrent, two-phase flow columns is mainly ascribed to viscous effects and molecular or eddy diffusion. Other factors causing axial mixing are drag from the motion of one of the counterflowing streams (large or small phase flow ratios), small density differences between phases, and maldistribution of the continuous and dispersed phases.

Although packings can to some extent reduce nonideal flow behavior (they minimize channeling by promoting transverse mixing), it is well established that under certain operating conditions (high flow rates, high pressure), severe axial mixing in either or both phases may occur. Unfortunately, available methods capable of describing quantitatively the extent of axial mixing in packed columns are limited in number, only giving an approximate description of the real mixing behavior. A large amount of axial data have been published in the literature for first-generation random packings (see the next section). For modern random packings (second generation) and structured packings, very few studies have appeared on axial mixing in gas–liquid flow (Kurtz et al., 1991; Mak et al., 1992).

In view of this lack of information, the present work was undertaken to provide experimental axial mixing data for both gas and liquid phases, using a dynamic response technique (tracer measurements), for second-generation random pack-

Correspondence concerning this article should be addressed to R. Macías-Salinas.
Present address for R. Macías-Salinas: Instituto Politécnico Nacional, ESIQIE-UPALM, Zacatenco, México, D.F. 07738.

ings and for structured packings, using a large-scale column. Such experimental mixing data will provide the first insight into the mixing behavior in modern packings as well as to assess the effect of axial mixing on interphase mass transfer in columns filled with such packings.

Previous Work

A number of experimental studies have been published on the mixing characteristics of two-phase flow through packed columns filled with first-generation random packings (Raschig rings and Berl saddles). To the best of our knowledge, however, only two publications have dealt with axial mixing in two-phase flow through beds of modern packings (Kurtz et al., 1991; Mak et al., 1992). Liquid has been investigated more extensively than gas mixing. Only a few studies are available on the latter (DeMaria and White, 1960; Sater and Levenspiel, 1966; Carleton et al., 1967; Dunn et al., 1977 and Kurtz et al., 1991). A survey of previous work reveals some important trends: axial mixing is greater in the liquid than in the gas, the response curves in the liquid show long tailing portions under trickle-flow conditions (Hoogendoorn and Lips, 1965; Sater and Levenspiel, 1966; Van Swaaij et al., 1969; Co and Bibaud, 1971; von Stockar and Cevey, 1984; Choe and Lee, 1985), and liquid mixing is unaffected by gas rate up to flood point (Otake and Kunugita, 1958; Polk and Clements, 1966; Sater and Levenspiel, 1966; Carleton et al., 1967; Bennett and Goodridge, 1970; Furzer and Michell, 1970; Co and Bibaud, 1971; Dunn et al., 1977; Furzer, 1984; Choe and Lee, 1985). In some studies end effects were effectively eliminated by the use of the two-point measuring technique (Sater and Levenspiel, 1966; von Stockar and Cevey, 1984; Choe and Lee, 1985; Mak et al., 1992).

Kramers and Alberda (1933) were among the first investigators to study axial mixing of two-phase flow in packed beds; they conducted a series of experiments on liquid-phase mixing with air and water flowing countercurrently through a bed of ceramic Raschig rings. Unlike other investigators, they found that liquid mixing was dependent on both gas and liquid flow rates. Otake and Kunugita (1958) studied liquid mixing for air–water using various columns filled with Berl saddles and Raschig rings of different sizes. They found that mixing decreased when bed length and/or interstitial liquid velocity increased or packing diameter decreased.

In the first reported study of gas mixing during two-phase flow, DeMaria and White (1960) described mixing experiments of air flowing through a wet packed column. They found gas mixing to increase with both gas and liquid rates. Hoogendoorn and Lips (1965) investigated the liquid mixing in gas–liquid flow through a packed column under bubble- and trickle-flow regimes. Their results for bubble flow indicate that the mixing coefficient of liquid is largely dependent on gas rate and nearly independent of liquid rate. In the case of trickle flow, they concluded that the strong tailing tendency of the response curves is likely due to liquid retained as static holdup.

Polk and Clements (1966) investigated liquid mixing characteristics for air–water flow through a randomly packed column. Unlike other investigators, they analyzed their data via frequency-domain fitting of the diffusion-type model, with good results. Using the imperfect-pulse technique along with a moments analysis, Sater and Levenspiel (1966) determined the extent of axial mixing in both gas and liquid. Their correlated mixing results for the gas (free of end effects) show a large disagreement when compared with those of DeMaria and White.

Carleton et al. (1967) conducted tracer tests in both phases for air–water flow through randomly packed columns of different diameters and under bubble-flow conditions. They found gas mixing to be higher in larger columns, but only slightly affected by packing size and liquid velocity up to 0.007 m/s. Their calculated liquid Péclet numbers (Pe) decreased with column diameter and packing size, and increased with liquid velocity (but were insensitive to gas velocity). Van Swaaij et al. (1969) reported the results of liquid residence-time distribution in packed columns under trickle-flow conditions. They observed that at small ratios of static holdup H_s to dynamic holdup H_d, mixing of the liquid was very small and comparable to the mixing at single-phase flow. They also found that at $H_d/H_s < 8$, the mixing increased as a result of the slow mass transfer between the stagnant regions and the mobile zones.

Bennett and Goodridge (1970) studied liquid axial mixing for gas–liquid flow through a randomly packed column with two different packing sizes and bed heights. They found the stagnant:dynamic liquid holdup to be independent of gas rate and to decrease with increasing liquid rate. Co and Bibaud (1971) found mixing in the liquid under trickle-flow conditions to be sufficiently described by a two-parameter mixing model such as the diffusion-type equation.

Dunn et al. (1977) developed empirical Péclet number correlations for both phases. They found that gas mixing decreases with increasing liquid or gas rates. Liquid Péclet numbers were found to be proportional to the liquid flow rate and insensitive to the gas rate. Farid and Gunn (1979) measured axial and radial mixing coefficients of the liquid under trickle and two-phase conditions. Their axial mixing coefficients are smaller than those of other workers who estimated coefficients for overall mixing without excluding wall-flow effects. They agreed with the long-standing axiom: when the ratio D_s/d_p is large, wall-flow effects can be neglected. They concluded that it is feasible to describe the mixing phenomena by the use of an effective mixing coefficient that includes the quantitative effect of local mixing and wall flow.

Burdett et al. (1981) measured static and dynamic holdup as well as axial mixing in a packed extraction column using light absorption. They found that static holdup decreased and dynamic holdup increased as dispersed-phase rate was increased at all continuous-phase rates. von Stockar and Cevey (1984) studied the effect of viscosity and surface tension on axial mixing and holdup of the liquid. They found no significant effect of surface tension on dynamic holdup and that liquid–phase mixing appeared to be independent of both viscosity and surface tension.

Choe and Lee (1985) obtained mixing and liquid holdup data in a packed column, and found that holdup decreased with increasing packing size and the liquid-phase Péclet number increased with both gas and liquid rates. Kurtz et al. (1991) offered a few residence time distribution data for gas with different liquid loadings: for air–water in Flexipac 2Y structured packing. They qualitatively showed the effect of liquid rate on the axial mixing of the gas.

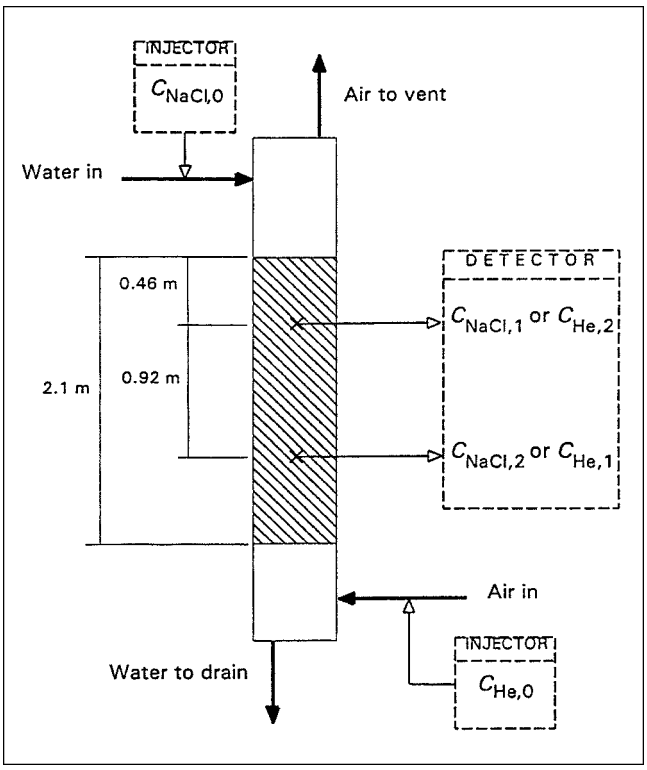

Figure 1. Experimental scheme for two-phase flow.

Mak et al. (1992) used a pulsed packed column and extended their earlier mixing data (Mak et al., 1991) by studying the mixing properties of the liquid during countercurrent contacting of a slurry flow through Sulzer SMV-12 structured packing. They observed that as the interstitial velocities of the solid–liquid mixture increased, the mixing coefficient increased. They found also that moderate pulsation velocities can reduce the slurry mixing to a minimum.

Tracer Experiments

Tracer measurements of air and water under two-phase flow conditions were made using a large-scale packed column (0.43 m diameter, 6.69 m high, with a 2.1 m packed section). Four packings were used: 25.4-mm ceramic Raschig rings (first generation), 25.4-mm metal Pall rings (second generation), Sulzer BX structured packing and Flexipac 2 structured packing. The structured packings contained wall wipers, which were adjusted to ensure a snug fit at the column wall. Wall wipers were not used with the random packings; however, the column:packing diameter ratio of about 16 is well above the recommended minimum of 8 to ensure absence of wall flow.

Water flowed countercurrently with air through the packing in forms of rivulets, drops or films at atmospheric pressure and ambient temperature. Details of the column, packing characteristics, pulse injection method, and two-point detection technique are described in Part I of this article (Macías-Salinas and Fair, 1999). Figure 1 shows the experimental scheme, based on the approach described.

An injection-detection system was built for each phase to allow both the introduction of imperfect pulses of a nonreactive tracer into the inlet stream and the measurement of the two response curves at the detection points. The inert tracers were helium in the gas and an aqueous solution of NaCl in the liquid; they were detected by thermal conductivity and electrical conductance, respectively. Macías-Salinas (1995) provides detailed information on the injection-detection system. The gas sampler, unlike that used in the single-phase flow experiments described in Part I, was equipped with a highly hydrophobic polytetrafluoroethylene (PTFE) membrane to obtain gas samples free of liquid.

For each water loading (3.25, 5, 6.75, and 8.5 kg/m^2-s), the air flow rate was increased until either flooding or excessive entrainment of water was visually observed at the column top section. Pressure-drop measurements of the gas were made in order to establish the operating limits of gas rates at each liquid loading (see Table 1). To confirm the linearity of the mixing measurements, the time of injection was varied (from 0.1 to 1 s for the gas, and from 1 to 2 s for the liquid).

Mixing Model

Both gas- and liquid-side dynamic response data were reproduced with the aid of the diffusion-type model (Eq. 1) with boundary conditions corresponding to an infinite bed or open system. The parameters characterizing the flow behavior (interstitial velocity v and effective mixing coefficient D_e) were determined for each pair of RTD curves using the same estimation methods described in Part I:

$$D_e \frac{\partial^2 C}{\partial z^2} - v \frac{\partial C}{\partial z} = \frac{\partial C}{\partial t}. \tag{1}$$

Other forms of the mixing parameters allowing an easier physical interpretation are the mean residence time,

$$\theta_m = \frac{L}{v} \tag{2}$$

and the dimensionless Bodenstein number,

$$Bo = \frac{vL}{D_e}. \tag{3}$$

From Eq. 3, one can see that the term D_e/v has units of length and represents the mean mixing path of the fluid elements passing through the bed. Accordingly, the Bo number can be defined in terms of the test-section length L (= 0.92

Table 1. Operating Limits of Gas Rates for Each Packing

Packing	Range of Gas Rates [kg/m^2·s]			
	$L = 3.25$*	$L = 5$	$L = 6.75$	$L = 8.5$
25.4-mm Raschig rings	0.5–1.61	0.5–1.5	0.5–1.25	0.25–1.125
25.4-mm Pall rings	1–3.76	1–3.3	1–2.83	1–2.56
Sulzer BX	1–3	1–2.41	1–2.2	1–2
Flexipac 2	1–4.65	1–4.14	1–3.68	1–3.49

*L in kg/m^2·s

m) and the mixing length L_{mix}:

$$Bo = \frac{L}{L_{mix}}. \tag{4}$$

Under plug flow conditions, there is no mixing, $L_{mix} = 0$, and Bo becomes infinity. At the other extreme, $L_{mix} = \infty$, corresponding to perfect mixing, with $Bo = 0$.

Results and Discussion

All the experimental response curves were reproduced using values of parameters θ_m and Bo obtained from the best estimation method. For all packings, both Fourier analysis and time-domain fitting produced the lowest root-mean-square errors (RMSE) between the experimental $C_{exp,2}$ and theoretical response curve $C_{cal,2}$. Accordingly, RMSE is defined by

$$\text{RMSE} = \left[\frac{\int_0^\infty \left(C_{exp,2} - C_{cal,2} \right)^2 dt}{\int_0^\infty \left(C_{exp,2} \right)^2 dt} \right]^{1/2}. \tag{5}$$

Gas-phase: Reproducibility of experimental response curves

Although the degree of spreading of the experimental response curves in the gas phase varied with both gas and liquid flow rates, their shapes remained almost Gaussian within the range of flow rates studied. Under these conditions, the diffusion-type model proved to be an excellent means for reproducing the experimental RTD curves, with an average RMSE value of 0.0198. The reproducibility results provided by each estimation method are similar to those under dry conditions (see Part I). Figure 2 shows the effect of gas rate on the shape of the RTD curves, measured at the second detection point, for 25.4-mm Raschig rings and a liquid loading of 3.25 kg/m^2-s. Even though the shapes of the RTD curves appear to be symmetrical, curve spreading increases as the flood point is approached, indicating an increased amount of mixing in the gas. Few measurements were made at high liquid rates because of experimental difficulties with the PTFE membranes used to collect gas samples free of liquid. The performance of the membrane was seriously affected by the increased accumulation of liquid inside the bed, particularly in the loading-to-flooding region, leading to water breakthrough. Similarly, Figure 3 shows the effect of the liquid rate on the tracer response curves for a given gas rate for the same packing. In this case the increase of the curve spreading is less pronounced, probably because of the slight variation of mean residence times of the gas with respect to liquid loading. For a range of flooding conditions, Figures 2 and 3 show that axial mixing in the gas is much more sensitive to the gas rate. Similar trends were also observed for the other packings.

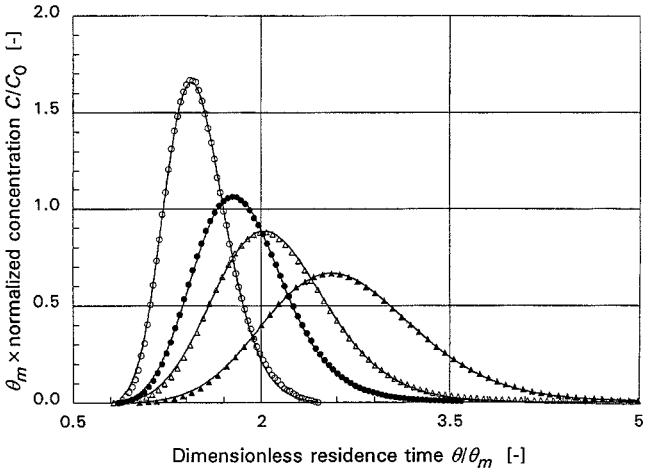

25.4-mm RASCHIG RINGS	Gas mass velocity [kg/m^2-s]
L_m = 3.25 kg/m^2-s	○ 0.5 (31% flood), θ_m = 1.4 s
Gas flow: Air	● 0.75 (47% flood), θ_m = 0.94 s
Tracer: Helium	△ 1.0 (62% flood), θ_m = 0.7 s
L = 0.9144 m	▲ 1.25 (78% flood), θ_m = 0.56 s

Figure 2. Effect of gas rate on the response curves in the gas at $L_m = 3.25$ kg/m^2·s.

The lines passing through the experimental points represent the theoretical curves predicted by the diffusion-type model.

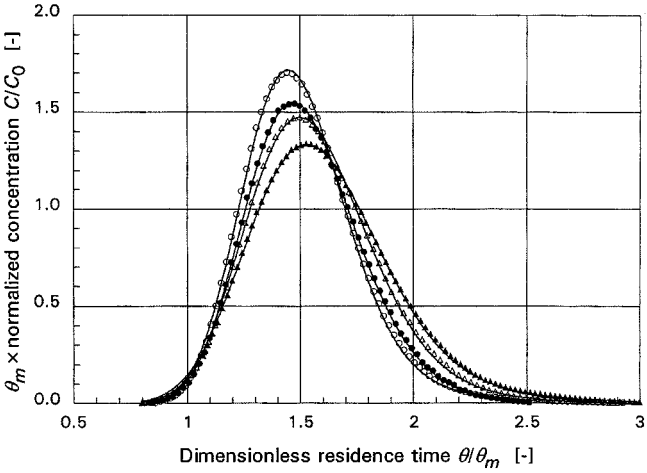

25.4-mm RASCHIG RINGS	Liquid mass velocity [kg/m^2-s]
G_m = 0.75 kg/m^2-s	○ 3.25 (47% flood), θ_m = 0.94 s
Gas flow: Air	● 5.0 (50% flood), θ_m = 0.91 s
Tracer: Helium	△ 6.75 (60% flood), θ_m = 0.91 s
L = 0.9144 m	▲ 8.5 (67% flood), θ_m = 0.9 s

Figure 3. Effect of liquid rate on the response curves in the gas at $G_m = 0.75$ kg/m^2·s.

The lines passing through the experimental points represent the theoretical curves predicted by the diffusion-type model.

Gas phase: Wet porosity and axial mixing results

The linearity of the mixing process was first verified by inspecting the dependence of the axial mixing coefficient D_e on

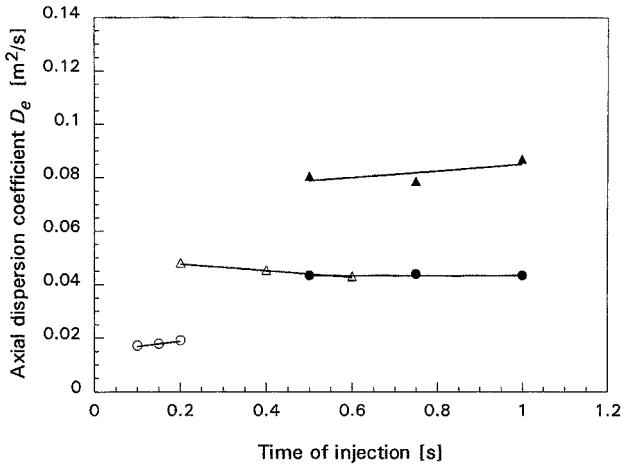

Gas flow: Air	○ 25.4-mm Raschig rings, G_m = 0.75 kg/m²-s
Tracer: Helium	△ 25.4-mm Pall rings, G_m = 2 kg/m²-s
D_t = 0.4286 m	● Sulzer BX, G_m = 1.75 kg/m²-s
L = 0.9144 m	▲ Flexipac 2, G_m = 2.5 kg/m²-s

Figure 4. Effect of time of injection on gas-phase dispersion coefficient D_e at $L_m = 8.5$ kg/m²·s.

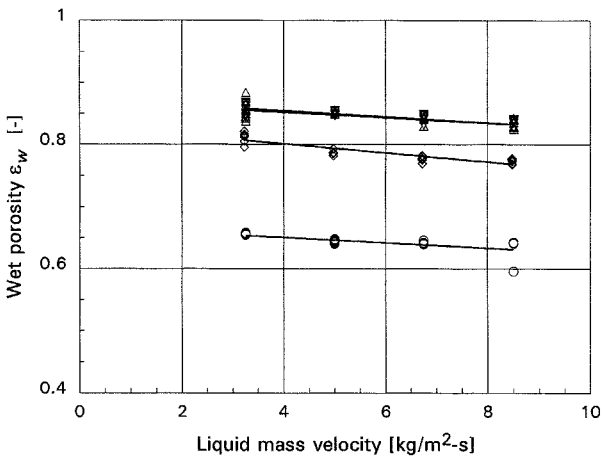

Gas flow: Air	○ 25.4-mm Raschig rings
Tracer: Helium	△ 25.4-mm Pall rings
D_t = 0.4286 m	◇ Sulzer BX
L = 0.9144 m	▽ Flexipac 2

Figure 5. Wet porosity vs. liquid rate at all gas rates.

the time of injection (amount of tracer injected). The results in Figure 4 show that the mixing coefficient for each packing changed very little with the amount of tracer injected, confirming the linearity of the flow system with respect to tracer concentration.

The mean residence time of the gas θ_m permitted calculation of the porosity of the wet packing ϵ_w, that is, the volume of the bed occupied by the gas under wet conditions:

$$\epsilon_w = \frac{\theta_m G_m}{L \rho_g} \tag{6}$$

where L is the test-section length. We found that the wet porosity appears to be more affected by liquid rate than by gas rate. As shown by Figure 5, the wet porosity decreases with increasing liquid loading for all four packings. The difference between the void fraction of the packing ϵ and the wet porosity ϵ_w should thus be regarded as the total holdup of the liquid phase:

$$H_t = \epsilon - \epsilon_w. \tag{7}$$

Accordingly, wet porosity at zero liquid flow rate can be related to the static portion of liquid holdup:

$$H_s = \epsilon - \epsilon_{w0}. \tag{8}$$

where ϵ_{w0} represents the intercept of the plot given in Figure 5 at $L_m = 0$. Consequently, the dynamic holdup is found to be

$$H_d = H_t - H_s = \epsilon_{w0} + \epsilon_w. \tag{9}$$

As expected, the total holdup values calculated from Eq. 7 are higher than those reported in Part I for liquid holdup without gas flow. The upflowing gas increases the local residence time of the liquid films, leading to an increase in liquid holdup.

The amount of axial mixing in the gas was found to increase with both gas and liquid rates for all four packings. As an example, Figure 6 shows mixing data for Flexipac 2. The

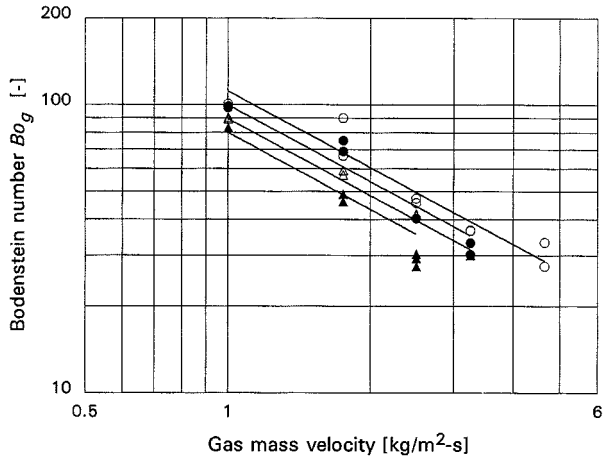

FLEXIPAC 2 Air-water flow system	Liquid mass velocity [kg/m²-s] ○ 3.25 ● 5 △ 6.75 ▲ 8.5
ε = 0.93, D_t = 0.43 m h = 2.1 m, L = 0.914 m	—— $Bo_g = 137.08 G_m^{-0.8835} \cdot 10^{-0.0276 L_m}$

Figure 6. Gas-phase Bodenstein number vs. gas rate, Flexipac 2.

experimental data exhibit considerable scatter because of the random nature of the measurements. The lines drawn through the points were obtained from a multiple regression analysis of the data using the correlating form:

$$Bo_g = \alpha' G_m^{\beta} \cdot 10^{\gamma' L_m}. \qquad (10)$$

The increased mixing in the gas at wet conditions results from the presence of the liquid within the bed, decreasing the void space and thus intensifying the turbulence of the gas in the flow channels. For this reason axial mixing levels for dry conditions (Part I) were markedly lower than those for the wet packing. Although the effect of liquid rate on the degree of mixing is evident, one should note that the mixing results obtained for the four packings were found to be strongly dependent on the gas rate. The power-law dependence between the mixing number *Bo* and the gas rate was found to be valid within the range of tracer measurements obtained. Near the flooding region, however, the assumption of this type of functionality is questionable. Nonuniform distribution of the gas appears to become more severe under high liquid loading conditions, that is, turbulence is more intense because of a wider variation of the shape and size of the flow channels. Under these conditions, the degree of mixing in the gas is expected to be significant. For most packings, however, it was difficult to determine the mixing behavior of the gas over the loading-to-flooding region because of gas sampler limitations.

Although the gas phase experiences more axial mixing under two-phase flow than at dry conditions, the levels of mixing found for each packing should be regarded as small-to-intermediate based on the mixing estimates previously given in Part I. Importantly, the contribution of the molecular diffusion coefficient D_m to the observed mixing phenomena is negligible because of the high gas rates used. Axial mixing is totally controlled by turbulent diffusion; the value of D_m (7×10^{-5} m^2/s) is much smaller than D_e, as is evident from Figure 4.

The extent of axial mixing in the gas greatly depends on the uniformity of gas distribution in the bed which, in turn, is coupled with the uniformity of liquid distribution to the bed. The liquid distributor used in this work is considered excellent, providing over 400 pour points/m^2. At liquid rates near the flood point, however, distribution of the phases may become nonuniform. The mixing results of each packing are plotted in Figure 7 for a gas rate of 1 kg/m^2-s and different liquid loadings. The high mixing levels shown by the Raschig rings may be attributed to the nonuniform distribution of the gas when approaching the flood point. On the other hand, the mixing results obtained for the high-porosity random packing (Pall rings) are comparable with those for the structured packings. This finding indicates that axial mixing in the gas phase is greatly affected by the wet porosity of the packing. For example, high-porosity packings having low levels of liquid holdup should sufficiently provide a wider range of gas rates at which axial mixing in the gas may be neglected. Also, gas distribution in this type of packing should remain uniform along the packed bed from low to moderate liquid rates.

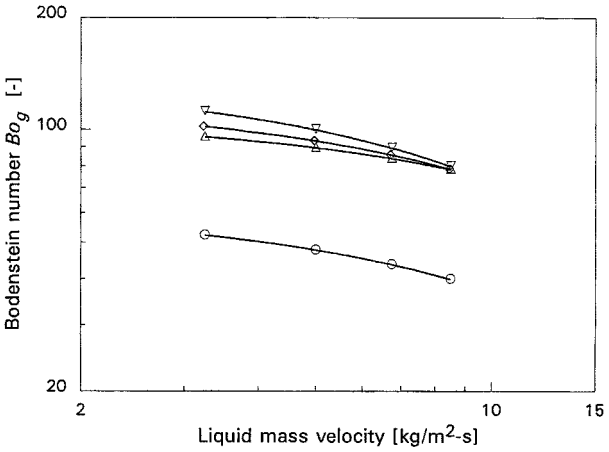

Figure 7. Gas-phase mixing numbers Bo_g vs. liquid rate as obtained from Eq. 10 at $G_m = 1$ kg/m^2·s.

Gas phase: Axial mixing correlations

A dimensional analysis was undertaken to express the present mixing results in terms of the major operating variables. The mixing numbers of both random packings were correlated via the use of a single expression by incorporating the effects of the packing geometry. The same geometrical group $d_p a_p$ used in Part I served to account for these differences in terms of size and shape. The following correlating form was therefore used to regress the data:

$$Bo_g = \alpha \left(\frac{G_m d_p}{\eta_g} \right)^{\beta} \cdot 10^{\gamma (L_m d_p)/\eta_l} (d_p \alpha_p)^{\varphi} \qquad (11)$$

or

$$Bo_g = \alpha Re_g^{\beta} \cdot 10^{\gamma Re_l} (d_p a_p)^{\varphi}. \qquad (12)$$

A multiple nonlinear regression analysis was performed on the data yielding,

$$Bo_g = 0.0878\, Re_g^{-0.8915} \cdot 10^{-0.00075 Re_l} (d_p a_p)^{8.231}, \qquad (13)$$

where the 95% confidence limits of the exponents β, γ, and φ are ± 0.0829, ± 0.00028, and ± 1.340, respectively. The preceding correlation acceptably reproduces the experimental data of both random packings within a $\pm 20\%$ difference between measured and predicted values.

The experimental mixing results of the two structured packings were also correlated using the form given by Eq. 12. The distinctive geometry of the structured packing motivated the use of the equivalent diameter d_{eq} of the flow channels as a characteristic length in the Reynolds numbers and the

geometrical factor:

$$Bo_g = \alpha\left(\frac{G_m d_{eq}}{\eta_g}\right)^{\beta} \cdot 10^{\gamma(L_m d_{eq})/\eta_l}\left(d_{eq} a_p\right)^{\varphi}. \qquad (14)$$

The value of the correlating constants was obtained by multiple nonlinear regression analysis of the data:

$$Bo_g = 4.2468 \times 10^8 Re_g^{-0.896} \cdot 10^{-0.00208 Re_l}\left(d_{eq} a_p\right)^{-7.792}. \quad (15)$$

A statistical analysis of this correlation provided the following 95% confidence limits of the exponents: $\beta \pm 0.0855$, $\gamma \pm 0.00062$, and $\varphi \pm 0.991$. Figure 8b indicates the difference between the observed and predicted values to vary over a $\pm 15\%$ range with moderate scatter.

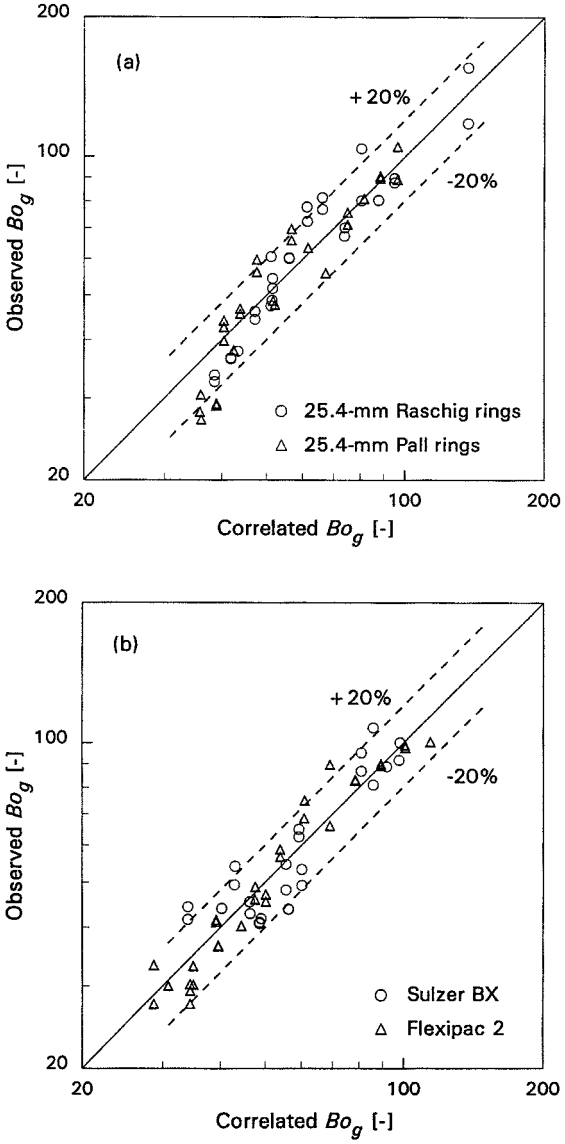

Figure 8. Comparison of experimental *Bo* numbers in the gas with values calculated by correlations (a) random packings (Eq. 13); (b) structured packings (Eq. 16).

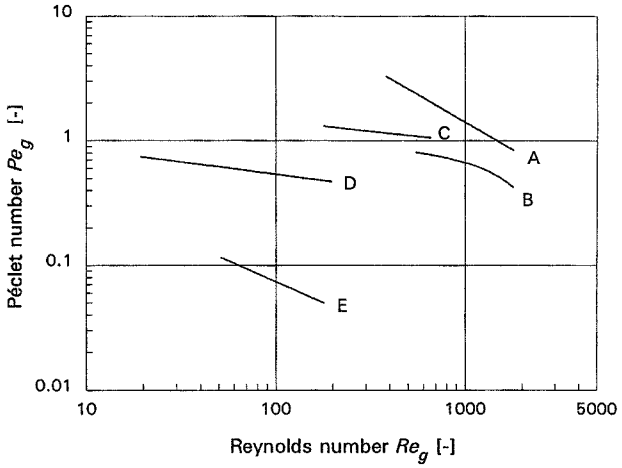

25.4-mm Raschig rings	12.7-mm Raschig rings
A: Present work	D: DeMaria & White (1960)
B: Dunn et al. (1977)	C: Sater & Levenspiel (1966)
C: Burghardt & Bartelmus (1979)	

Figure 9. Results from this work vs. gas-phase Péclet numbers from correlations by other authors at $Re_l = 125$ (12.7-mm Raschig rings) and $Re_l = 250$ (25.4-mm Raschig rings).

For the random packings, several earlier studies have been made with 25.4 ceramic Raschig rings. To compare the present correlated results with those previously reported, Eq. 13 has been expressed in terms of the gas Péclet number plus Reynolds numbers (Re) of both phases:

$$Pe_g = 998.19 Re_g^{-0.8811} \cdot 10^{-0.000812 Re_l}. \qquad (16)$$

Figure 9 shows gas Péclet numbers estimated from Eq. 16 and those calculated from earlier correlations, for a given liquid Reynolds number and two sizes of Raschig rings. There is reasonable agreement for the 25.4-mm rings, but considerable variation for the smaller rings. All the correlations agree in predicting a decrease in the gas Péclet number with an increase in the gas Reynolds number. The disagreement may be attributed to basic differences in experimental technique and methods of data analysis.

Liquid phase: Reproducibility of experimental response curves

As for single-phase flow, the liquid RTD curves in two-phase flow also showed strong tailing tendencies. But in contrast to the single-phase results, there was a larger experimental scatter of the tracer pulses for two-phase flow resulting from the presence of gas bubbles inside the sampling section of the conductance cells. The diffusion-type model served to reproduce the experimental data with satisfactory results (average RMSE value of 0.0511) despite the strong asymme-

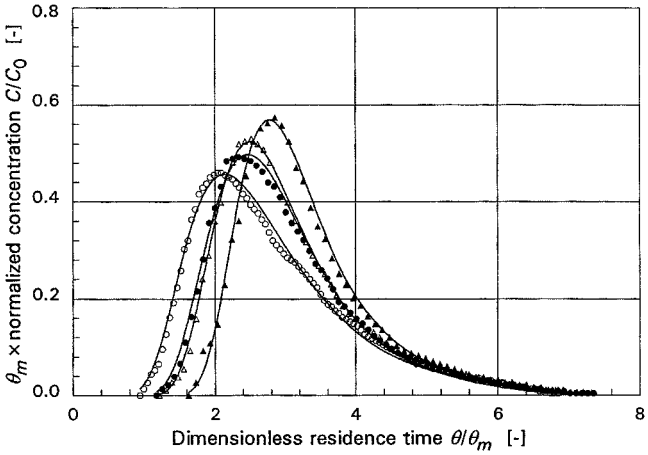

FLEXIPAC 2	Liquid mass velocity [kg/m^2-s]
G_m = 1.75 kg/m^2-s	○ 3.25 (38% flood), θ_m = 14.1 s
Liquid flow: Water	● 5.0 (42% flood), θ_m = 9.3 s
Tracer: NaCl	△ 6.75 (47% flood), θ_m = 8.9 s
L = 0.9144 m	▲ 8.5 (50% flood), θ_m = 7.3 s

Figure 10. Effect of liquid rate on the response curves in the liquid at $G_m = 1.75$ kg/m^2·s.

The lines passing through the experimental points represent the theoretical curves predicted by the diffusion-type model.

try of the response curves. As shown by Figure 10, there is a clear influence of liquid rate on response curve shape for Flexipac 2 structured packing at a fixed gas rate. As the liquid rate increases, the shape of the response curves becomes less asymmetric, indicating a smaller extent of mixing. At low liquid rates, the asymmetry (tailing) of the curves is more pronounced, probably as a result of increased liquid stagnation within the packing voids. Consequently, the degree of mixing would be expected to increase as the liquid load decreases. The dynamic response data in Figure 10 indicate that plug flow is approached as the liquid rate increases.

Figure 11 shows the effect of gas rate on the shape of the liquid-phase tracer curves at a constant liquid flow rate and for different approaches to flood. Although there is no regular progression indicated, it appears that as flooding is approached by increasing gas rate, the degree of mixing in the liquid decreases. One might have expected the opposite effect.

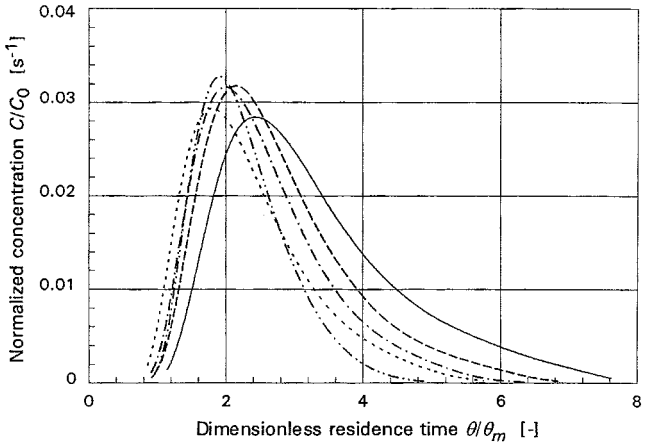

FLEXIPAC 2	Gas mass velocity [kg/m^2-s]
L_m = 3.25 kg/m^2-s	——— 1 (22% flood), θ_m = 12.8 s
	- - - - - 1.75 (38% flood), θ_m = 14.4 s
Liquid flow: Water	—·—·— 2.5 (54% flood), θ_m = 15.1 s
Tracer: NaCl	····· 3.25 (70% flood), θ_m = 17.7 s
L = 0.9144 m	—··—··— 4.312 (93% flood), θ_m = 20.1 s

Figure 11. Effect of gas rate on the response curves in the liquid at $L_m = 3.25$ kg/m^2·s.

The lines represent the best fit of the experimental data given by the diffusion-type model.

Liquid phase: total holdup and axial mixing results

The fraction of the bed occupied by the liquid (total holdup H_t) for countercurrent flow was evaluated from the mean residence times of the tracer curves. For example, calculated values of total holdup for 25.4-mm metal Pall rings have been plotted in Figure 12 for different approaches to flood, with liquid rate as a parameter. The present holdup results confirm observations by others in the sense that below the load point (about 70% of flood) liquid holdup is not significantly dependent on gas rate but only on liquid loading and packing geometry. Above the load point, liquid accumulation in the bed is strongly affected by gas rate, as observed by others from simple holdup experiments.

The lines passing through the experimental points were obtained from a multivariable regression analysis of the data based on the following equation:

$$H_t = \alpha' L_m^{\beta} \cdot 10^{\gamma' G_m}. \qquad (17)$$

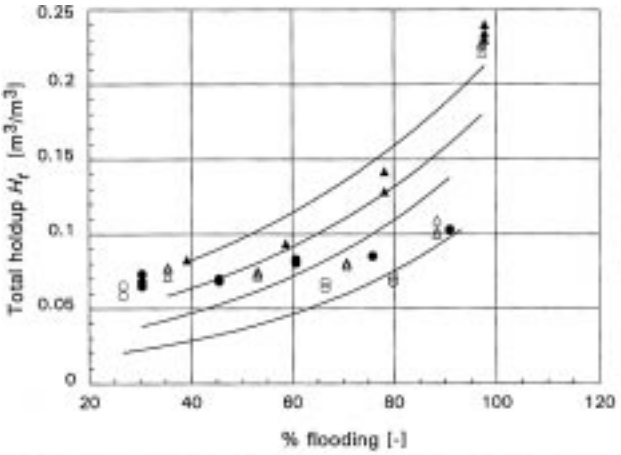

25.4-mm PALL RINGS Air-water flow system	Liquid mass velocity [kg/m^2-s]
ε = 0.94, D_t = 0.43 m h = 1.98 m, L = 0.914 m	○ 3.25 ● 5 △ 6.75 ▲ 8.5 —— $H_t = 0.00205 L_m^{1.42} \cdot 10^{0.028 G_m}$

Figure 12. Effect of gas flooding condition on the total holdup of the liquid, 25.4-mm Pall rings.

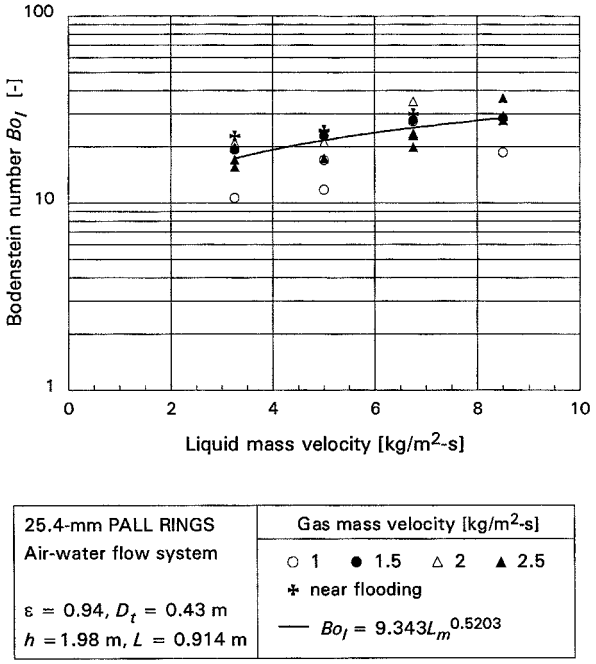

Figure 13. Liquid-phase Bodenstein numbers vs. liquid rate, 25.4-mm Pall rings.

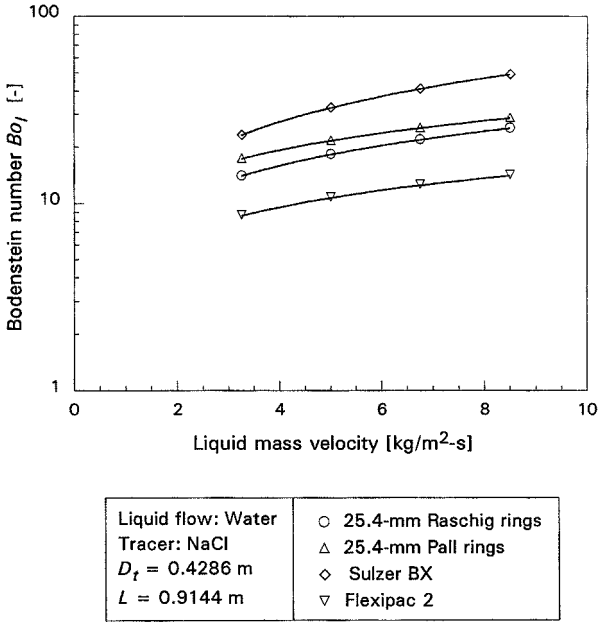

Figure 14. Correlated mixing numbers in the liquid as a function of liquid rate.

As evidenced by Figure 12, the fit of Eq. 17 to the data is poor because of the complex influence of gas rate on liquid holdup in the loading-to-flooding region. The transition between preload and loading conditions can be abrupt, as studied by Verschoof et al. (1999), and holdup equations show a discontinuity at the transition. In the loading-to-flooding region the behavior of liquid holdup and pressure drop of the gas under wet conditions are somewhat similar because of their interrelationship by interfacial shear.

It was not possible to confirm the linearity of the mixing process because of the large amount of experimental scatter of the liquid-phase mixing data. As in the case of single-phase trickle flow, axial mixing in the liquid decreases with increasing liquid rate. Figure 13 shows this functionality for the Pall rings under a range of gas rates. The cause of the data scatter is not completely clear, but in part results from the difficulty in locating the truncation point in the tailing portion of the response curves. It can be deduced that the effect of gas rate is essentially negligible in the range investigated, compared with the data scatter, which in turn reflects fluctuations of liquid flow through the packing. It can be noted that as the flood point is approached, mixing levels in the liquid are unaffected by the gas rate. This agrees with the finding of Furzer (1984), who measured liquid mixing properties of several random packings operating near the flood point.

For the four packings studied, the dependence of the liquid Bodenstein number on liquid rate was found to be approximately the same. A power-law relationship between these two quantities sufficiently described the results within the range of liquid rates studied:

$$Bo_l = \alpha' L_m^{\beta}. \tag{18}$$

Within the range of liquid rates, axial mixing in the liquid phase for two-phase flow is principally caused by hydrodynamic effects rather than by molecular behavior. The molecular diffusivity of the liquid (1.6×10^{-9} m^2/s) is much smaller than the axial mixing coefficients observed. The range of Bodenstein numbers for two-phase flow (6 to 60) is indicative of intermediate-to-large mixing levels in the liquid phase based on estimates of the degree of mixing made by Levenspiel (1972). This indicates that there is more axial mixing in the liquid than in the gas under the present experimental conditions.

Figure 14 shows the comparison of liquid mixing for the four packings, based on correlated data provided by Eq. 18. Sulzer BX produced the lowest mixing results; this was expected because of the excellent wettability properties of the gauze material, resulting in uniform spreading of liquid on the packing surface. As a result, mixing of the liquid between adjacent sheets is minimized, leading to minimal mixing in the axial direction. A somewhat surprising result was obtained for Flexipac 2, which produced the highest amount of mixing in the liquid, as evidenced by Figure 14. This is in agreement, however, with observations of Suess and Spiegel (1992) and Verschoof et al. (1999), who attribute the mixing to accumulation at the intersections between packing elements, accentuated by the sharpness of the 45-deg corrugation angle (the Sulzer BX has a 60-deg angle). Other possible causes: poor wetting of the packing surface in the range of liquid rates investigated, thus increasing the length of mixing of the liquid films due to their irregular paths through the flow channels, and high levels of turbulence in the films caused by the grooved surface of the packing. The liquid accumulation at the junctions of adjacent packing elements is likely the major cause of liquid mixing.

While the trends of the present mixing results with or without gas flow are the same, their values vary notably in magni-

tude. Mixing levels for two-phase flow are lower than those of single-phase flow for the majority of the packings, with the exception of the Raschig rings (see Part I). In general, the countercurrent effect of gas flow is to promote uniformity of the liquid films leading to a reduction of the length of mixing of the fluid elements. Also, the presence of gas flow in the channels tends to reduce or eliminate local mixing between liquid films flowing on adjacent packing elements or sheets. These observations, however, fail to explain the adverse effect of the gas rate on the mixing results obtained for the Raschig rings. It is likely that the high turbulence in the liquid films caused by the tortuous flow paths and the low porosity of the packing explains these results.

Liquid phase: axial mixing correlations

The correlating forms proposed in Part I for single-phase trickle flow have also been used to correlate the present experimental results for two-phase flow (mixing behavior in both cases depends on the liquid flow pattern and packing geometry). The liquid-phase Bodenstein numbers for the two random packings were correlated as a function of the liquid rate and packing geometry according to

$$Bo_l Ga^{1/3} = \alpha \left(\frac{L_m d_p}{\eta_l} \right)^{\beta} \left(d_p a_p \right)^{\gamma} = \alpha Re_l^{\beta} \left(d_p a_p \right)^{\gamma}, \quad (19)$$

where the Galileo group Ga remained fairly constant and was not considered as a correlating variable in the preceding equation. By a nonlinear regression analysis of the data, the following correlation results:

$$Bo_l = 24.461\, Re_l^{0.5544} Ga^{-1/3} \left(d_p a_p \right)^{2.1127}, \quad (20)$$

with 95% confidence limits of the exponents β and γ being equal to ± 0.1609 and ± 1.4577. As shown by Figure 15a, there is a fair agreement between the correlated and experimentally determined values of Bo_l with a maximum $\pm 20\%$ of difference for most of the data.

Because of the vast availability of earlier studies on liquid-phase axial mixing through 25.4-mm ceramic Raschig rings, the correlated results obtained obtained for this packing were compared to those published by previous investigators. For this purpose, Eq. 20 has been written in terms of the Péclet number and the Reynolds number of the liquid phase:

$$Pe_l = 0.0244\, Re_l^{0.6138} \quad (21)$$

Figure 16 shows the comparison of the results provided by this equation with results obtained by other correlations. Evidently, there is a significant disagreement among the different correlations using the same size and type of packing. The values of the Péclet number calculated by Eq. 21 are not appreciably different from those correlated by von Stockar and Cevey (1984), who used the two-point technique to eliminate end effects as well as a modified method of moments to avoid overweighting the tailing portion of their experimental RTD curves. The small difference between these two correlations

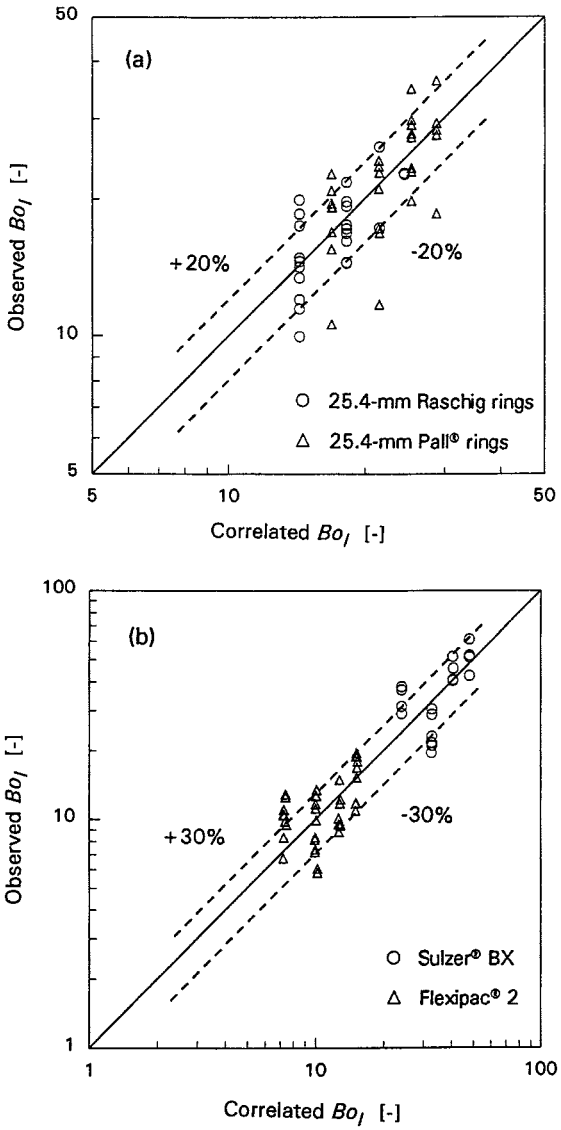

Figure 15. Comparison of experimental *Bo* numbers in the liquid with values calculated by correlations (a) random packings (Eq. 20); (b) structured packings (Eq. 23).

results from von Stockar and Cevey varying liquid properties to ascertain their effects on axial mixing. On the other hand, the correlations of Dunn et al. (1977) and Co and Bibaud (1971) give values of the Péclet number comparable to those predicted by the correlations of Sater and Levenspiel (1966) and Choe and Lee (1985) based on a smaller size of Raschig rings (12.7 mm). Since axial mixing increases with decreasing size of the packing, it can be deduced that the correlations of Dunn et al. and Co and Bibaud overestimate by far the amount of mixing in 25.4-mm ceramic Raschig rings because of their failure to exclude end effects from the tracer measurements.

For structured packings, the major correlating variables affecting the liquid-phase mixing are liquid flow rate L_m, inclination angle ϕ of the channels with respect to the horizontal,

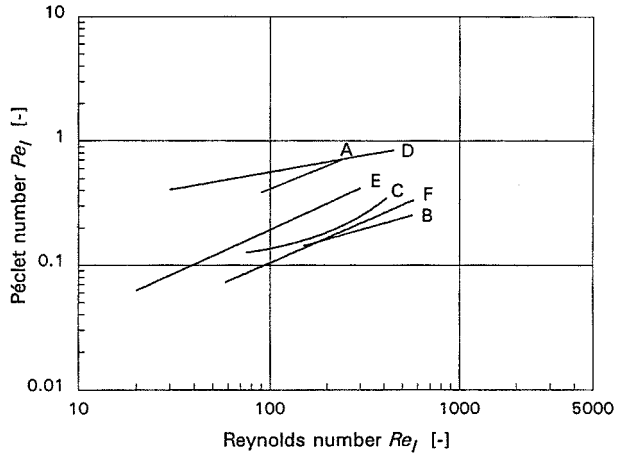

A: Present work	D: von Stockar & Cevey (1984)
B: Co & Bibaud (1971)	E: Sater & Levenspiel (1966), 12.7-mm RR
C: Dunn et al. (1977)	F: Choe & Lee (1985), 12.7-mm RR

Figure 16. Results of this work vs. liquid-phase Péclet numbers computed from correlations of other authors (12.7- and 25.4-mm Raschig rings).

and the size of the flow channels d_{eq}. These variables have been incorporated into a correlating form described in Part I:

$$Bo_l = \alpha \left(\frac{\eta_l L_m}{d_{eq}^2 \rho_l^2 g} \right)^{\beta} \left(\frac{3}{\sin^2\phi} \right)^{\gamma} (d_{eq} a_p)^{\varphi}. \qquad (22)$$

The correlation obtained via a multiple nonlinear regression analysis of the data is given by

$$Bo_l = 8.154 Fi^{0.7082} \left(\frac{3}{\sin^2\phi} \right)^{1.159} (d_{eq} a_p)^{6.337}, \qquad (23)$$

where the 95% confidence limits of the preceding exponents are 0.7082 ± 0.2061, 1.159 ± 0.7756, and 6.337 ± 2.7735. As shown in Figure 15b, agreement between the measured and calculated Bo_l values is only fair.

Conclusions

Axial mixing properties of air and water in countercurrent flow were determined via dynamic response experiments for a second-generation random packing and two structured packings using a large-scale column. Gas and liquid holdup data were also obtained. The conclusions drawn from the present study are:

- The results follow the same mixing trends reported previously for first-generation random packings. Axial mixing in the gas increases with both gas and liquid rates, whereas axial mixing in the liquid decreases with increasing liquid rate and is insensitive to gas rate.

Table 2. Qualitative Rank-Order Comparison of Mixing Level for Four Packings Studied

Level of Axial Mixing	Two-Phase Flow	
	Gas Phase	Liquid Phase
Highest (low *Bo*)	RR1	FLEX2
	PR1	RR1
	SULBX	PR1
Lowest (high *Bo*)	FLEX2	SULBX

Note: RR1 = 25.4-mm Raschig rings, PR1 = 25.4-mm Pall rings, SULBX = Sulzer BX, FLEX2 = Flexipac 2.

- The experimental RTD curves in both phases are adequately reproduced by the diffusion-type model. For larger amounts of mixing (longer tails of the response curves), the diffusion-type model may be unable to predict the effect of liquid stagnancy in the packing voids. In this case a flow model containing a capacitance term such as the PDE model (Villermaux and Van Swaaij, 1969; Bennett and Goodridge, 1970; Stepanek and Shilimkan, 1973) should provide a more complete flow response description.
- A qualitative comparison of the mixing performance of the four packings under the present experimental conditions is presented in Table 2. The results show that on an overall basis Sulzer BX produces the least axial mixing in both phases, because of its uniform wet porosity and excellent wettability. The large gas mixing found for the Raschig rings results from increased turbulence levels in the gas flow. The high liquid mixing level for Flexipac 2 is attributed largely to discontinuities at the intersection of adjacent packing elements.
- The following correlations were developed in terms of dimensionless quantities for the prediction of axial mixing in both phases under countercurrent, two-phase flow conditions:

For random packings (25.4-mm Raschig rings and 25.4-mm Pall rings):

$$Bo_g = 0.0878\, Re_g^{-0.8915} \cdot 10^{-0.00075 Re_l} (d_p a_p)^{8.231} \qquad (24)$$

$$Bo_l = 24.461\, Re_l^{0.5544} Ga^{-1.3} (d_p a_p)^{2.1127}; \qquad (25)$$

valid operating ranges:

$$340 < Re_g < 4066$$

$$90 < Re_l < 237$$

$$1.79 \times 10^8 < Ga < 1.93 \times 10^8$$

$$4.83 < d_p a_p < 5.21.$$

For structured packings (Sulzer BX and Flexipac 2):

$$Bo_g = 4.2468 \times 10^8 Re_g^{-0.896} \cdot 10^{-0.00208 Re_l} (d_{eq} a_p)^{-7.792} \qquad (26)$$

$$Bo_l = 8.154 Fi^{0.7082} \left(\frac{3}{\sin^2\phi} \right)^{1.159} (d_{eq} a_p)^{6.337}; \qquad (27)$$

Table 3. Standard Deviations of Mixing Correlations

Equation	SD_{Bo}	Number of points N
24	7.843	52
25	7.437	56
26	4.013	54
27	5.596	58

$$SD_{Bo} = \sqrt{\frac{1}{N-1}\sum_{i=1}^{N}(Bo_{\text{cal}} - Bo_{\text{exp}})_i^2}$$

valid operating ranges:

$$381 < Re_g < 3516$$

$$25 < Re_l < 122$$

$$1.53\times10^{-6} < Fi < 1.59\times10^{-5}$$

$$3.16 < d_{eq}a_p < 3.53$$

$$45° < \phi < 60°.$$

The standard deviations SD_{Bo} of Bo_g and Bo_l using the preceding equations are given in Table 3. The correlating forms for the liquid-phase Bodenstein number given by Eqs. 25 and 27 completely differ, thus reflecting the distinctive liquid mixing mechanisms occurring in random and structured packings. There is a fair agreement between correlated and experimentally determined values of Bo within $\pm 22\%$ of difference for most of the data.

• Equations 24 through 27 can be conveniently used in a more rigorous efficiency model to predict quantitatively the effect of axial mixing on interphase mass transfer in two-phase flow columns filled with modern packing. This will prove to be an essential diagnostic tool in order to confirm or invalidate the assumption of plug flow conditions.

Acknowledgments

The authors thank the Separations Research Program at The University of Texas at Austin, and the National Council of Science and Technology of México (CONACyT) for providing financial support for this research.

Notation

a_p = packing surface area, m^2/m^3
C = tracer concentration, kg/m^3
C_0 = total tracer concentration integrated over all time, $(kg/m^3)\cdot s$
d_p = nominal diameter (random packing), m
D_t = column diameter, m
Fi = film number, $\eta_v/d_{eq}^2\rho g$
g = acceleration due to gravity, m/s^2
G_m = gas flow rate, $kg/m^2\cdot s$
L^* = characteristic length, m
t = time, s
v_s = superficial velocity, m/s
z = axial distance coordinate, m

Greek letters

α = regression constant
α' = regression constant, $(kg/m^2\cdot s)^{-\beta}$
β = regression constant
γ = regression constant,
γ' = regression constant, $(kg/m^2\cdot s)^{-1}$
η = viscosity, $kg/m\cdot s$
φ = regression constant
ρ = density, kg/m^3

Subscripts

cal = predicted value
exp = measured value
g = gas phase
l = liquid phase
p = packing
1 = first measuring point
2 = second measuring point

Literature Cited

Bennett, A., and F. Goodridge, "Hydrodynamic and Mass Transfer Studies in Packed Absorption Columns. Part I: Axial Dispersion," *Trans. Inst. Chem. Eng.*, **48**, T232 (1970).

Burdett, I. D., D. R. Webb, and G. A. Davies, "A New Technique for Studying Dispersion Flow, Holdup and Axial Mixing in Packed Extraction Columns," *Chem. Eng. Sci.*, **36**, 1915 (1981).

Burghardt, A., and G. Bartelmus, "Experimental Determination of Longitudinal Dispersion in Two-Phase Flow through Packing," *Chem. Eng. Sci.*, **34**, 405 (1979).

Carleton, A. J., R. J. Flain, J. Rennie, and F. H. H. Valentin, "Some Properties of a Packed Bubble Column," *Chem. Eng. Sci.*, **22**, 1839 (1967).

Choe, D. K., and W. K. Lee, "Liquid Phase Dispersion in a Packed Column with Countercurrent Two-Phase Flow," *Chem. Eng. Commun.*, **34**, 295 (1985).

Co, P., and R. Bibaud, "Longitudinal Mixing of the Liquid Phase in Packed Columns with Countercurrent Two Phase Flow," *Can. J. Chem. Eng.*, **49**, 727 (1971).

DeMaria, F., and R. R. White, "Transient Response Study of Gas Flowing Through Irrigated Packing," *AIChE J.*, **6**, 473 (1960).

Dunn, W. E., T. Vermeulen, C. R. Wilke, and T. T. Word, "Longitudinal Mixing in Packed Gas-Absorption Columns," *Ind. Eng. Chem. Fundam.*, **16**, 116 (1977).

Farid, M. M., and D. J. Gunn, "Dispersion in Trickle and Two-Phase Flow in Packed Columns," *Chem. Eng. Sci.*, **34**, 579 (1979).

Furzer, I. A., "Axial Liquid Dispersion in Countercurrent Gas-Liquid Reactors near the Gas Flooding Condition," *Ind. Eng. Chem. Fundam.*, **23**, 159 (1984).

Furzer, I. A., and R. W. Michell, "Liquid-Phase Dispersion in Packed Beds with Two-Phase Flow," *AIChE J.*, **16**, 380 (1970).

Hoogendoorn, C. J., and J. Lips, "Axial Mixing of Liquid in Gas-Liquid Flow Through Packed Columns," *Can. J. Chem. Eng.*, **43**, 125 (1965).

Kramers, H., and G. Alberda, "Frequency Response Analysis of Continuous Flow Systems," *Chem. Eng. Sci.*, **2**, 173 (1958).

Kurtz, D. P., K. J. McNulty, and R. D. Morgan, "Stretch the Capacity of High-Pressure Distillation Columns," *Chem. Eng. Prog.*, **87**, 43 (1991).

Levenspiel, O., *Chemical Reaction Engineering*, 2nd ed., Wiley, New York (1972).

Macías-Salinas, R., "Gas- and Liquid-Phase Axial Dispersion Through Random and Structured Packing," PhD Diss., The University of Texas at Austin, Austin (1995).

Macías-Salinas, R., and J. R. Fair, "Axial Mixing in Modern Packings, Gas and Liquid Phases: I. Single-Phase Flow," *AIChE J.*, **45**, 222 (1999).

Mak, A. N. S., C. A. J. Koning, P. J. Hamersma, and J. M. H. Fortuin, "Axial Dispersion in Single-Phase Flow in a Pulsed Packed Column Containing Structured Packing," *Chem. Eng. Sci.*, **46**, 819 (1991).

Mak, A. N. S., P. J. Hamersma, and J. M. H. Fortuin, "Solid Holdup and Axial Dispersion During Countercurrent Solids-Liquid Contacting in a Pulsed Packed Column Containing Structured Packing," *Chem. Eng. Sci.*, **47**, 565 (1992).

Otake, T., and E. Kunugita, ''Mixing Characteristics of Irrigated Packed Towers,'' *Chem. Eng. Jpn.*, **22**, 144 (1958).
Polk, E. M., and W. C. Clements, ''Liquid Phase Dynamics of a Packed Absorption Column Using Pulse Testing Methods,'' *Vanderbilt Univ. Tech. Rep. No. 10*, Vanderbilt Univ., Nashiville, (1966).
Sater, V. E., and O. Levenspiel, ''Two-Phase Flow in Packed Beds. Evaluation of Axial Dispersion and Holdup by Moment Analysis,'' *Ind. Eng. Chem. Fundam.*, **5**, 86 (1966).
Stepanek, J. B., and R. V. Shilimkan, ''Residence Time Distribution in an Axially-Dispersed Plug Flow with Capacity,'' *Trans. Inst. Chem. Eng.*, **51**, 112 (1973).
Suess, P., and L. Spiegel, ''Hold-Up of Mellapak Structured Packings,'' *Chem. Eng. Proc.*, **31**, 119 (1992).
Van Swaaij, W. P. M., J. C. Charpentier, and J. Villermaux, ''Residence Time Distribution in the Liquid Phase of Trickle Flow in Packed Columns,'' *Chem. Eng. Sci.*, **24**, 1083 (1969).
Verschoof, H. J., Z. Olujic, J. R. Fair, ''A General Correlation for Predicting the Loading Point of Corrugated Sheet Structured Packings,'' *Ind. Eng. Chem. Res.*, **38**, 3663 (1999).
Villermaux, J., and W. P. M. Van Swaaij, ''Modèle Représentatif de la Distribution des Temps de Séjour dans un Réacteur Semi-Infini à Dispersion Axiale avec Zonez Stagnantes. Application à l'Écoulement Ruisselant dans de Colonnes d'Anneaux Raschig,'' *Chem. Eng. Sci.*, **24**, 1097 (1969).
Von Stockar, U., and P. F. Cevey, ''Influence of the Physical Properties of the Liquid on Axial Dispersion in Packed Columns,'' *Ind. Eng. Chem. Process Des. Dev.*, **23**, 717 (1984).

Manuscript received Feb. 16, 1999, and revision received Aug. 18, 1999.